Sustainable Energy & Fuels

Ultrathin Alumina Passivation for Improved Photoelectrochemical Water Oxidation Catalysis of Tin Oxide Sensitized by a Phosphonate-Functionalized Perylene Diimide First Without, and Then With, CoOy

Journal:	*Sustainable Energy & Fuels*
Manuscript ID	SE-ART-06-2021-000908.R1
Article Type:	Paper
Date Submitted by the Author:	20-Aug-2021
Complete List of Authors:	Finke, Richard; Colorado State University, Chemistry Jewell, Carly; Colorado State University Subramanian, Ashwanth ; Stony Brook University, Materials Science and Chemical Engineering; Brookhaven National Laboratory, Center for Functional Nanomaterials Nam, Chang-Yong; Brookhaven National Laboratory, Center for Functional Nanomaterials

Ultrathin Alumina Passivation for Improved Photoelectrochemical Water Oxidation Catalysis of Tin Oxide Sensitized by a Phosphonate-Functionalized Perylene Diimide First Without, and Then With, CoO_y

Carly F. Jewell, [†] Ashwanth Subramanian, [#] Chang-Yong Nam, [*, ‡, #] Richard G. Finke[*,†]

[†]Department of Chemistry, Colorado State University, Fort Collins, Colorado, 80523, United States

[‡]Center for Functional Nanomaterials, Brookhaven National Laboratory, Upton, New York, New York 11973, United States

[#]Department of Materials Science and Chemical Engineering, Stony Brook University, Stony Brook, New York 11794, United States

Abstract

Previously, a photoanode composed of nanostructured SnO_2 coated with the perylene diimide dye N,N′-bis(phosphonomethyl)-3,4,9,10-perylenediimide (PMPDI) plus photoelectrochemically deposited cobalt oxide (CoO_y) was shown to photoelectrochemically oxidize water at 31 ± 7% Faradaic efficiency. A non-ideal part of that prior system is that the addition of the known CoO_y water oxidation catalyst (WOC) resulted in a *reduction* of the total photocurrent rather than the anticipated increase, due to an increase in charge-carrier recombination. Herein, we show deposition of an ultrathin alumina overlayer applied by atomic layer deposition (ALD) on the SnO_2/PMPDI photoanode can improve the photoactivity and catalytic activity of the system; the addition a ca. 1-nm-thick AlO_x layer deposited on a *4000 nm (i.e., 4 micron) thick mesoporous* anode system can and does have a positive, 2.5-fold improvement in the steady-state photocurrent with 29 ± 9% Faradaic efficiency vs the control anode without alumina passivation by reducing charge-carrier recombination. Moreover, ALD-deposited AlO_x layer does help support the understanding of the "anti-catalysis" of co-depositing a CoO_y WOC on the SnO_2/PMPDI DS-PECs—specifically the picture of direct CoO_y–SnO_2 contact-mediated recombination—but was unable to improve the photocurrent in a net SnO_2/PMPDI/AlO_x(/CoO_y) system. We attribute the lack of a performance enhancement by CoO_y WOC to incomplete

coverage of each SnO_2 nanoparticle by the AlO_x. Overall, we find the addition of an optimized *ultrathin* AlO_x layer (0.6 nm thick; deposited at 85 °C) improves the SnO_2/PMPDI/AlO_x system's photoactivity by a factor of up to ca. 3-fold with reduced recombination. These results document that metal-oxide passivation by low-temperature ALD can be an effective strategy for improving the water oxidation performance of even nanostructured dye sensitized-photoelectrochemical cell.

Introduction

Efficient photoelectrochemical solar water splitting into molecular hydrogen and oxygen is one of the must-solve problems in chemistry[1,2] en route to fulfilling the growing global demand for clean, renewable energy while minimizing CO_2 emissions.[3–7] Recently, the application of *organic* dyes as light absorber for solar water splitting has drawn extensive attention due to their relatively low cost, their production from earth-abundant materials, the ease of processability, and the ability to synthetically tailor the organic dye as needed en route to optimized water-splitting performance.[4,8] Previously, we developed a first,[9] then a second[10] generation water-oxidation photoanode using both organic thin-film and dye-sensitized photoelectrolysis cell (OTF-PEC and DS-PEC) architectures based on a perylene diimide dye derivative (N,N´-bis(phosphonomethyl)-3,4,9,10-perylenediimide, PMPDI, Figure 1) and a co-deposited CoO_y water oxidation catalyst (WOC).[11–13] PDIs have high light-absorption extinction coefficients (ca. 22,000 M^{-1} cm^{-1} at λ_{max} of 500 nm for PMPDI[10]) and are used in industrial settings as both car paints and in plastics.[8] PDIs are further attractive as the light-gathering component in water-oxidation catalysis (WOCatalysis) devices due to their high thermal stability[14], high oxidative stability both in air and in water, and due to their resistance to photobleaching under even extreme conditions, including hypochlorite solutions.[15]

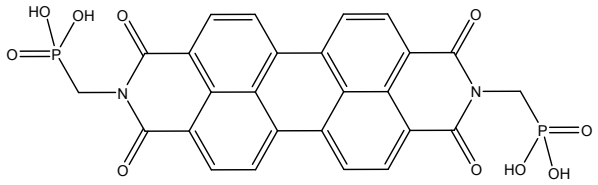

Figure 1. Molecular structure of PMPDI

As for the WOC component, CoO_y is an earth-abundant, heterogeneous, prototype WOC.[16] Our previous study on the PMPDI OTF-PEC architecture showed a 10-fold enhancement of water-oxidation photocurrent by applying co-deposited CoO_y as the WOC[9], but the system exhibits a low light-harvesting efficiency (LHE) (ca. 12% at λ_{max}) and a large amount of charge carrier recombination, with only 6% charge transport efficiency.[9] An optimized second-generation PMPDI DS-PEC system architecture consisting of nanostructured SnO_2 coated with PMPDI is able to achieve a LHE of >99% at λ_{max} and a charge transport efficiency of 13%.[10] However, it was found that the same CoO_y WOC, necessary to produce oxygen, in fact *decreased* the water oxidation performance in the second-generation SnO_2/PMPDI/CoO_y system relative to the first.[9,10] That unexpected, undesired, "anti-catalyst" behavior was attributed to increased charge recombination between photoinjected electrons in the SnO_2 conduction band and accumulated holes in CoO_y at the SnO_2 surface.[10,17,18] More generally, that "anti-catalyst" behavior illustrates the acknowledged broader challenge[19] of coupling water-oxidation as well as others catalysts to light-absorbing units in ways that minimizes charge-carrier recombination back reactions.

To begin to address the forefront question of how to best couple catalysts and light-adsorbing units, we previously attempted to improve the performance of SnO_2/PMPDI/CoO_y DS-PECs by using a wet chemical method[10] to deposit a thin layer of electronic insulator AlO_x on the SnO_2 surface as an established tunneling barrier[17,20] against recombination. That effort led to an improved photovoltage, but a reduced photocurrent due to a hindered charge injection between the dye and SnO_2.[10]

In related work, Kamire et al. reported reduced charge recombination by applying 0.5 – 3 nm thick ultrathin AlO_x coating directly over dyes by atomic layer deposition (ALD) in a DS-PEC system consisting of nano-TiO_2 sensitized by perylene monoimide (PMI) dye.[21] The observed decreased recombination was attributed to the passivation of recombination-active TiO_2 surface states and to an increased barrier for tunneling-based recombination with redox-active species in solution.[21] The addition of the AlO_x layer further served to stabilize the dye, resulting in improved device lifetimes. Significantly, those workers observed that the addition of an Ir-dimer-based WOC resulted in a ca. 66% *reduction* of photocurrent, both with and without the AlO_x overlayer[21], closely analogous to what we have observed in our previous study where the addition of the known WOC[16] CoO_y decreased the photocurrent output of SnO_2/PMPDI DS-PEC.[10] These examples make

apparent the forefront problem of effectively coupling the DS-PEC systems to desired catalysts such as a WOC without, instead, enhancing undesirable recombination. These studies further suggest the hypothesis that the performance of DS-PECs and catalysts may be improved if the recombination passivation layer can be further optimized to also allow the WOC to function as desired.

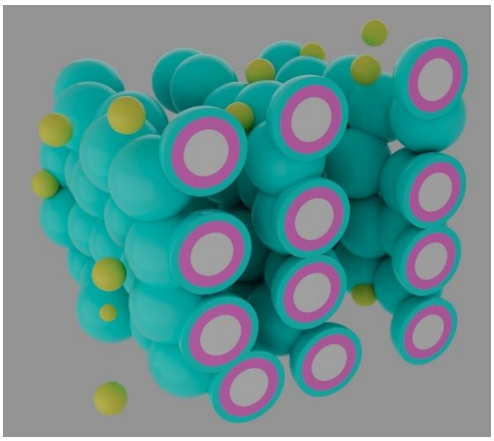

Figure 2. Idealized structural models of the SnO_2/PMPDI/AlO_x/CoO_y anode where SnO_2 is grey, PMPDI is pink, AlO_x is blue, and CoO_y is yellow. Nanostructured SnO_2 is reflective of SEM images that will be presented in a figure later in the paper.[10] Anode notation throughout is written in order of deposition, left to right (ie SnO_2 is deposited first, followed by PMPDI, then AlO_x, and then finally CoO_y).

Herein, we explore the impact of adding an insulating AlO_x layer prepared by ALD onto PMPDI-sensitized nanostructured SnO_2 DS-PECs on their solar water splitting performance, idealized by Figure 2. More specifically, we address two primary questions via the ALD approach: (i) can the deposition of an ultrathin alumina overlayer applied by ALD on the PMPDI/SnO_2 photoanode improve the photoactivity and catalytic activity of the CoO_y WOC? More specifically, (ii) can the addition of a 0.6 to 1.3 nm thickness AlO_x layer have any measurable, much less useful effect, on a *4000 nm (i.e., 4 micron) thick and also nanoporous* anode system? If so, (iii) what are the effects of key parameters on the photo- and catalytic-activity, notably the layer thickness and deposition temperature of the alumina overlayer? (iv) Can a better, ALD-controlled deposition of an ultrathin AlO_x layer address the carrier recombination issues of SnO_2/PMPDI DS-PECs, and (v) can the ultrathin, ALD-deposited AlO_x layer probe, and perhaps even improve our understanding of why co-deposited CoO_y WOC on the SnO_2/PMPDI DS-PECs has, to date, resulted in a decreased, "anti-catalysis" photocurrent? Herein we investigate the effects of ultrathin

AlO_x thickness (0.6 – 1.3 nm) and ALD temperature applied to a 4 μm thick DS-PEC photoanode system on the overall anode photoactivity, device/organic dye stability, and, importantly, the catalytic activity of CoO_y WOC by characterizing the system's open-circuit photovoltage, photocurrent, and O_2 product yield and hence Faradaic efficiency under solar PEC water splitting conditions. The results allow insights into the five questions posed that form the basis for the present research. In addition, the studies which follow make apparent when and how ALD-deposited alumina layers should or should not be used to try to improve analogous DS-PECs, the needed considerations of layer thickness, and factors to be considered when using ALD on nanostructured devises. The results provide a working hypothesis for going forward about how to couple WOC and other catalysts to DS-PECs for improved catalyst efficiency.

Experimental

Materials. The following starting materials and solvents were used as received to generate buffer solutions: KOH (Fisher, Certified ACS grade, 98.5%, 1.5% water, 0.00028% Fe, 0.0008% Ni); KH_2PO_4 (Fisher, Certified ACS Grade, 99.3%, 0.0005% Fe); hydroquinone (Aldrich, >99%); NANOpure water (Barnstead NANOpure ultrapure water system, 18.0 MΩ). NANOpure water was used for all experiments.

Synthesis of PMPDI dye, and the deposition of SnO_2 anode and CoO_y WOC. All synthetic and manufacturing details for PMPDI dye and the SnO_2 anodes can be found in our previous publications[9,10]. Briefly, the anodes are composed of fluorine-doped tin oxide (FTO)-coated glass as a transparent current collector, covered by a mesoporous SnO_2 film, sensitized with PMPDI, and CoO_y WOC. All fabricated photoanodes have SnO_2 film with "2-Scotch" layer thickness conditions[10] where PMPDI dyes were loaded for 24 hr at 95 °C from a saturated solution of fully protonated PMPDI in water.[10] CoO_y WOC was added to photoanodes by photoelectrochemical deposition[9,10]; the anodes (SnO_2/PMPDI or SnO_2/PMPDI/AlO_x) were submerged in a solution of pH 7, 0.5 mM $Co(NO_3)_2$ and 0.1 M potassium phosphate butter (KPi) and held at +0.2 V vs Ag/AgCl under 1 sun illumination for 3 min.[10] Anodes were then rinsed with water for 30 s and allowed to air dry.

Ultrathin AlO_x coating by ALD. Ultrathin conformal AlO_x layer was deposited on PMPDI or glass substrate using a Cambridge Nanotech Savannah S100 ALD system (base pressure ~ 0.4

Torr). The deposition temperature was set at 85 °C; PMPDI was shown to be stable up to 400 °C herein. The depositions were carried out by sequential exposure of trimethyl aluminum (TMA) (14 ms) and water vapor (40 ms) with an intermediate purge time of 60 s for both precursors. Spectroscopic ellipsometry was used to calibrate the AlO_x thickness per ALD cycle using Si control substrates and found a linear growth rate of 0.067 nm per cycle (Figure S1 and Table S1; see Supporting Information for details). The number of ALD cycles was varied between 4 and 28 to deposit AlO_x on SnO_2/PMPDI or glass substrates ranging between 0.4 and 2.0 nm, respectively. In a separate set of experiments, the ALD temperature has been varied from 85, 150, and to 200 °C to investigate the impact of deposition temperature on the device performance. AlO_x deposition was verified using scanning electron microscopy (SEM) imaging and X-ray photoelectron spectroscopy (XPS) methods, *vide infra*.

Photoelectrochemical testing. All photoelectrochemical experiments were done in a previously decribed[10] custom two-compartment Pyrex cell consisting of a working compartment (1 × 1.5 × 1.5 cm^3, 5 ml) and an auxiliary compartment separated by a medium porosity glass frit. Experiments were conducted using a CH Instruments CHI630D potentiostat, a Pt wire counter electrode positioned in the auxiliary compartment and a Ag/AgCl (3 M NaCl, +0.215 V vs normal hydrogen electrode (NHE)) reference electrode positioned in the working compartment in close proximity to the anode surface. The anode was clamped with an alligator clip to the front wall of the working compartment with the uncoated, nonconductive glass side pressed against the cell wall. The cell was filled with ca. 5 ml electrolyte (pH 7, 0.1 M KPi buffer) sufficient to cover the film. The anode was illuminated from the substrate side using a 65 W xenon arc lamp (PTO model A1010), which was powered by an OLIS XL150 adjustable power supply. The light passed through a bandpass filter (315 – 710 nm, Thorlabs KG3, FGS900S) and an ultraviolet (UV) filter (400 nm long-pass, Thorlabs FGL400S). The power density of the light was adjusted to reflect the visible region of the airmass 1.5 global (AM 1.5G) spectrum.[10] In the experiments in which transients (interrupted illumination) of 5 s or 30 s were used, a manual shutter was used to block the light.[10] Each anode was tested with a series of electrochemical experiments in the order detailed below. First the cell was allowed to short-circuit in the dark for 60 s to depopulate the electrons from SnO_2 sub-bandgap states.[10] The 60 s was determined to be a sufficient length of time to depopulate the excited state as the current reached a steady-state within 15 s. Then the open-circuit potential, V_{oc}, was measured vs the Ag/AgCl reference electrode for 90 s in the dark and then

measured again under illumination for 90 s. Next, a photocurrent transient experiment was performed in which the anode was held at +0.2 V vs Ag/AgCl for 300 s with 30 s light/dark transients throughout. A potential of +0.2 V vs Ag/AgCl was chosen for photocurrent transient experiments as photocurrent is fully saturated by this applied potential. The cell was again allowed to short-circuit in the dark for 60 s, and the V_{oc} in both the dark and light were remeasured. Then the current-voltage (*i-V*) photocurrent transient experiment was performed. The voltage was scanned from -0.2 to +1.0 V vs Ag/AgCl with a 10 mV/s scan rate and 5 s light transients. Each experiment was reproduced a minimum of three times with three separate anodes produced under identical conditions. All figures and values reported herein are representative of the photoactivity of the system indicated. Care was taken to ensure that the reported results are reproducible and not due to a defective anode or otherwise irreproducible sample.

IPCE and APCE Determinations. Incident photon to current efficiency (IPCE) measurements were calculated from action spectra collected using a Xe arc lamp (Oriel model 66002, calibrated to approximate the AM1.5 reference power in the visible region), power supply (Oriel model 68700), monochromator (Oriel Cornerstone 130, model 7400), and a CH Instruments 630D potentiostat. All experiments were run in the presence of 20 mM H_2Q sacrificial agent in pH 7 0.1 M KPi buffer using the same two-compartment Pyrex cell used for all photoelectrochemical testing; a Pt wire counter electrode positioned in the auxiliary compartment and a Ag/AgCl (3 M NaCl, +0.215 V vs normal hydrogen electrode (NHE)) reference electrode positioned in the working compartment in close proximity to the anode surface were again used. In order to collect the action spectra, the electrode being test was held at +0.2 V vs Ag/AgCl while incident monochromatic light (ca. 3 nm bandwidth) was scanned from 400 to 700 nm across 25 nm intervals. A silicon standard power sensor (Thorlabs model S120B) was used to measure the incident lamp power through the same aperture at each wavelength, P_{mono}. Photocurrent, I_{ph}, was measured at each wavelength by recording the photocurrent during three 15 second light transients and subtracting off any dark current. The average photocurrent was then used to calculate the IPCE according to equation 1:

$$\mathrm{IPCE}(\lambda) = \frac{I_{ph}(\mathrm{mA}) \times 1239.8\ (\mathrm{V \cdot nm})}{P_{mono}(\mathrm{mW}) \times \lambda(\mathrm{nm})} \qquad \text{eq. 1}$$

The absorbed-photon-to-current efficiency (APCE) was calculated by dividing the light harvesting efficiency (LHE)—i.e., the absorptance spectrum measured from the anode—out of the IPCE, using equation 2. Note that the APCE is equivalent to the injection efficiency, ϕ_{inj}, multiplied by the charge collection efficiency, η_{col}.

$$\mathrm{APCE} = \frac{\mathrm{IPCE}}{\mathrm{LHE}} = \phi_{inj}\eta_{col} \qquad \text{eq. 2}$$

Oxygen detection. Oxygen yield was experimentally measured using the generator–collector (G-C) technique detailed elsewhere:[10,22–24] photoanode 'generators' were sandwiched with an FTO "collector",[10] separated by a Parafilm spacer. A CH Instruments CHI-750D bipotentiostat was used for the G-C experiments. The G-C cell was placed in the previously detailed working compartment with the generator side against the wall of the cell with the incoming light. The cell was filled with pH 7, 0.1 M KPi buffer, approximately 10 ml, which was degassed with Ar for a minimum of 30 min. An Ag/AgCl (3 M NaCl) electrode was used as a reference and was also placed in the working compartment. A Pt wire was used as a counter electrode and was placed in the auxiliary compartment. Current was measured at both the generator and collector electrodes, which were held at +0.2 V and −0.65 V vs Ag/AgCl, respectively. The current was collected for 300 s in the dark, 300 s in the light, then 300 s in the dark in order to ensure that all oxygen had diffused across the two electrodes and that all current attributable to oxygen production was collected. Control experiments with FTO/CoO_y anodes were used to determine the collection efficiency of the sandwich configuration and used to calculate the O_2 yield and Faradaic efficiency of each photoanode.

Results and Discussion

The effects of AlO_x overlayer on the photoelectrochemical activity of SnO_2/PMPDI

As noted in the Introduction, the addition of an electronically insulating metal-oxide shell layer over the mesoporous semiconductor substrate (and sometimes the dye as well) has been shown to reduce recombination and increase photocurrents in dye-sensitized systems.[17,20,21,25–32] In a previous study, 1.3 nm thick metal oxide deposited at 85 °C was found to be optimal for a photoanode system based on organic semiconductor thin films.[28] Hence, as to start and as a

baseline, a 1.3 nm thick layer of AlO_x was deposited at 85 °C by ALD onto the previously optimized[10] PMPDI-sensitized mesoporous SnO_2.

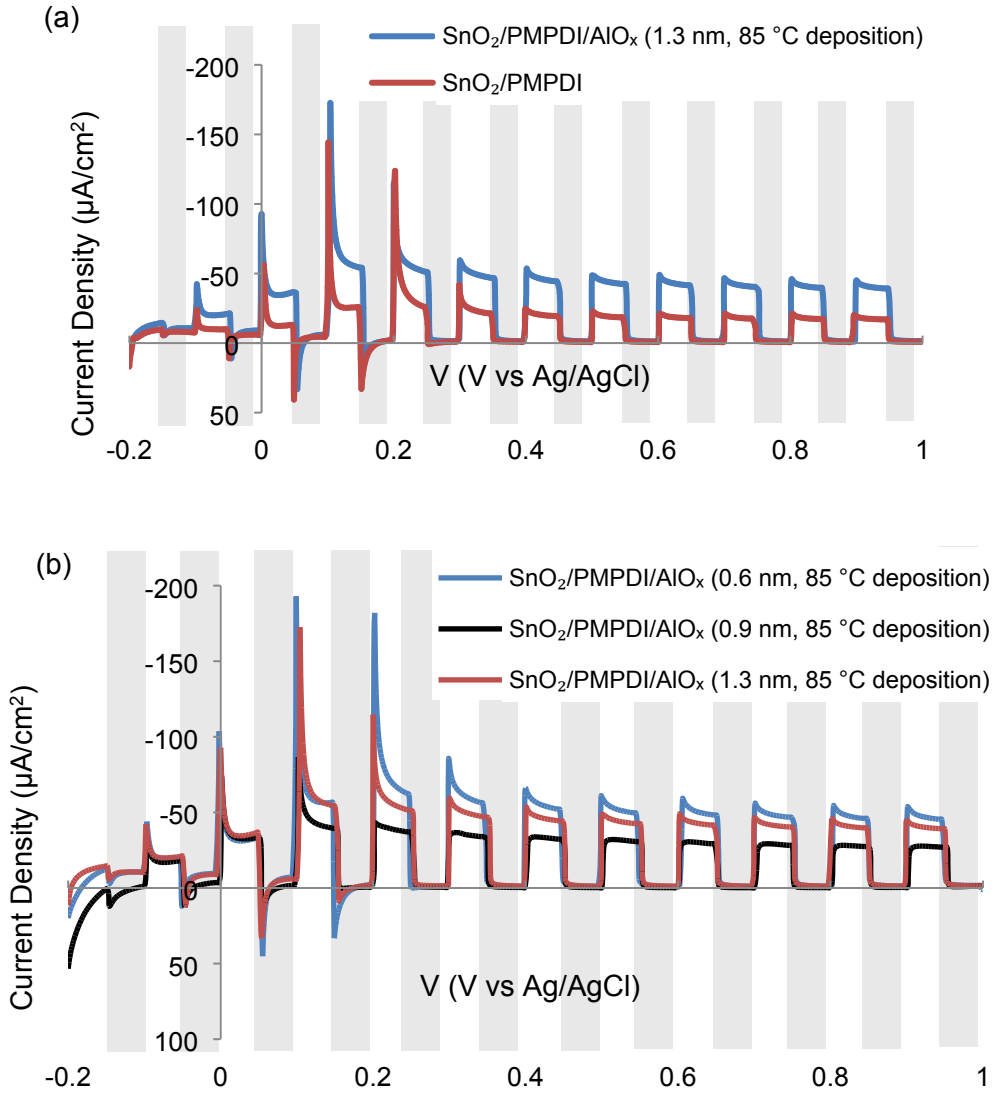

Figure 3. Photocurrent transients (indicated by light (light-on)/ dark (light-off) shading, 5 s each) collected in pH 7, 0.1 M KPi electrolyte for: (a) SnO_2/PMPDI/AlO_x (1.3 nm, 85 °C deposition temperature, blue) and SnO_2/PMPDI (red) anodes.; (b) SnO_2/PMPDI/AlO_x (0.6 nm, 85 °C deposition, blue), SnO_2/PMPDI/AlO_x (0.9 nm, 85 °C deposition, black) and SnO_2/PMPDI/AlO_x (1.3 nm, 85 °C deposition, red) anodes. Comparatively thinner, 0.6 nm, layers of alumina yield higher photocurrents than the 0.9 and 1.3 nm counterpart.

Photoactivity was recorded for each anode in tested in a scanning voltammetry experiment coupled with light/dark phototransients (Figure 3a). Working from left to right, the voltage is scanned from −0.2 to +1.0 V vs Ag/AgCl with a 10 mV/s scan rate. For each of the phototransients, illumination of the photoanode causes a rapid rise in anodic (negative y-axis) current and then blocking of the light each 5 s causes the rapid drop in current. The large current spikes observed at ca. +0.1 V vs Ag/AgCl are also present on bare SnO_2 anodes,[10] indicating that the spikes cannot fully be attributed to PMPDI, but are likely related to SnO_2 recombination centers.[10,17]

We find that by the addition of the 1.3 nm of AlO_x overlayer deposited at 85 °C, SnO_2/PMPDI/AlO_x, significantly increased both peak and steady-state photocurrent by approximately 1.6-fold and 2.5-fold, respectively, compared with the system without any AlO_x (Figure 3a). The increased peak and steady-state photocurrents suggest that the charge carrier production/collection is increased, likely due to a reduced carrier recombination. Note, the deposition of AlO_x has negligible effect on the absorptance spectrum of the SnO_2/PMPDI electrode (Figure S2) and alumina itself was shown not to produce significant photocurrent on its own, indicating that AlO_x is likely not functioning as a major WOC (Figure S3). The addition of AlO_x also reduces the ratio of peak to steady-state anodic photocurrent (i.e., current 'spiking' behavior), which is often attributed to charge recombination caused by metal-oxide surface states.[10,17,33–35] The SnO_2/PMPDI system displayed ca. 87% anodic decay from peak to steady-state photocurrent over 5 min at +0.2 V vs Ag/AgCl, while the SnO_2/PMPDI/AlO_x decayed slightly less, ca. 76%. This spiking behavior can also be indicative of photocorrosion due to excessive charging of the light absorber.[36] Photocorrosion is certainly an issue in tough oxidative reactions, such as water splitting, and as such these same experiments were carried out using hydroquinone (H_2Q) (Figure 4). With the addition of hydroquinone, the spiking behavior is minimized, suggesting that the more kinetically and thermodynamically facile reaction can outrun the recombination pathways. In short, increasing the desirable kinetic pathways with the addition of H_2Q can overcome the recombination pathways. Overall, these observations are consistent with the partial passivation of surface trap states on SnO_2 and PMPDI by 1.3 nm thick AlO_x.

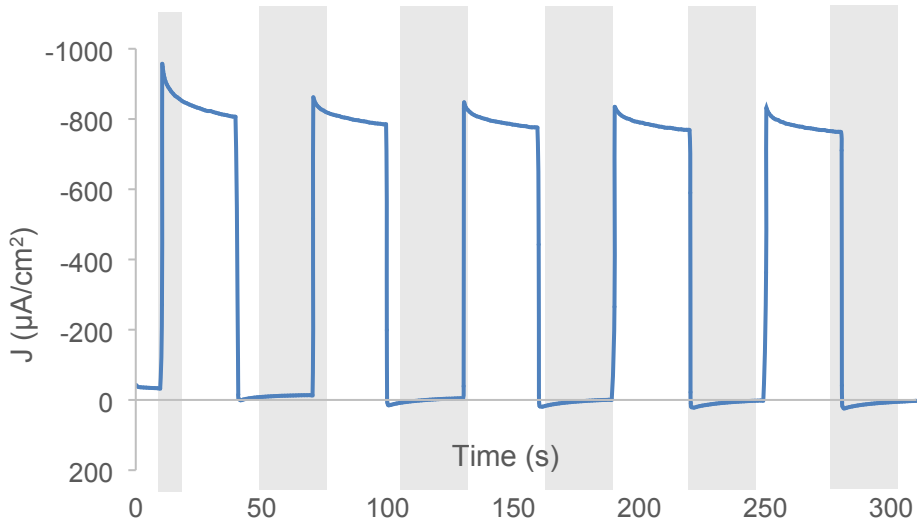

Figure 4. Photocurrent transients (with 30 s light/dark intervals) for a representative SnO_2/PMPDI/AlO_x/CoO_y (0.6 nm, 85 °C deposition) anode. Transients were performed at +0.2 V vs Ag/AgCl in pH 7, 0.1 M KPi buffer with 20 mM H_2Q. Background H_2Q currents were subtracted off.

To maximize the device performance enhancement by the AlO_x anode passivation layer, it is necessary to optimize the thickness of AlO_x that balances its benefits (e.g., surface state passivation and reduced carrier recombination) with the possible decrease in photoactivity from an ineffective charge transfer between the semiconductor to electrolyte, a decreased surface area, or separation of the dye from the catalyst, all of which can be caused by a too thick AlO_x overlayer. Alumina is an insulator and hence functions as a tunneling barrier. Finding a balance between moving charge carriers through the AlO_x and fully covering the SnO_2 is fundamentally important to minimizing recombination while maintaining charge carrier movement, that is to say optimizing the kinetics. However, there is largely inconsistent information in the literature as to the optimal thickness of ALD overlayer in DS-PEC systems, with reports ranging from sub-monolayer to 3 nm.[21,25,28,37–42] Therefore, a series of anodes with varying overlayer thicknesses from 0.6 nm to 1.3 nm were investigated (Figure 3b) in order to determine the thickness at which the kinetics are optimized, which will be discussed herein and is detailed below in Scheme 1. We find that the photocurrent was maximized with relatively thinner AlO_x layer, reaching, for example, −182 μA/cm^2 at +0.2 V vs Ag/AgCl for 0.6 nm AlO_x, compared with −64 and −115 μA/cm^2 for 0.9 nm and 1.3 nm thick AlO_x, respectively. This result illustrates that an even modestly thicker AlO_x passivation layer can indeed interfere with the charge transfer between the anode and electrolyte, consistent with previous literature.[43]

As illustrated in Figure 3, we find that the photocurrent spiking behavior still exists regardless of the AlO_x passivation thickness. Considering that photocurrent spiking is often attributed to metal oxide surface trap states,[10,33,35,44] we tested if increasing the AlO_x deposition temperature could affect the spiking behavior, since higher AlO_x ALD temperature should in principle result in the growth of more stochiometric Al_2O_3 with reduced defect density and increased coating uniformity.[45–50,51] X-ray photoelectron spectroscopy (XPS) was done in in an attempt to detect distinct environments between the alumina depositions, but no differences were observed (Figure S4). Specifically, SnO_2/PMPDI anodes were coated with 0.6 nm of AlO_x at 85 °C, 150 °C, and 200 °C, and their photoelectrochemical activities were compared (Figure 5). Interestingly, the increased AlO_x ALD temperature resulted in a rather minor increase in the extent of photocurrent spiking, while *decreasing* the overall photocurrent. To quantify the photocurrent spiking behavior, we calculate the percentage of photocurrent decay from peak to steady state measured at +0.2 V vs Ag/AgCl from each system. The SnO_2/PMPDI/AlO_x systems with AlO_x deposited at 85, 150, and 200 °C displayed a photocurrent decay of ca. 76%, 84%, and 83%, respectively. In the meantime, the photocurrent peak decreased from −182 μA/cm^2 at +0.2 V vs Ag/AgCl for the AlO_x deposited at 85 °C to −107 and −92 μA/cm^2 for the AlO_x deposited at 150 and 200 °C, respectively. However, regardless of deposition temperature, the addition of AlO_x overlayer still yielded a higher photocurrent than the neat PMPDI, consistent with the role of AlO_x mitigating as desired against charge carrier recombination.

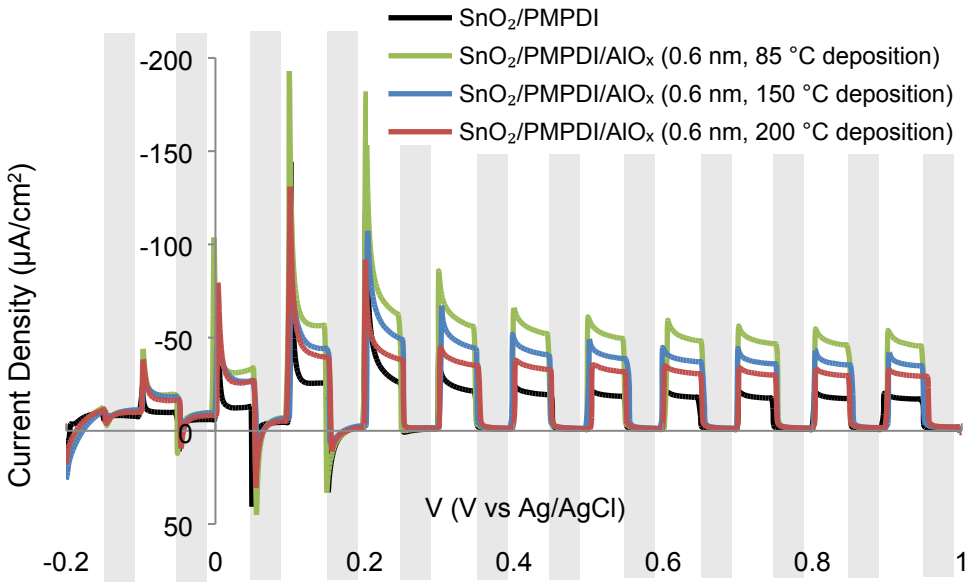

Figure 5. Photocurrent transients (indicated by light (light-on)/ dark (light-off) shading, 5 s each) collected in pH 7, 0.1 M KPi electrolyte for SnO_2/PMPDI (black), SnO_2/PMPDI/AlO_x, (0.6 nm, 85 °C deposition, green), SnO_2/PMPDI/AlO_x, (0.6 nm, 150 °C deposition, light blue), and SnO_2/PMPDI/AlO_x, (0.6 nm, 200 °C deposition, red) anodes. Scans were run from −0.2 to +1.0 V vs Ag/AgCl. Increasing the deposition temperature of AlO_x yielded a decrease in photocurrent.

A control experiment was performed to show that the decrease in photocurrent at higher AlO_x ALD temperature is not caused by the thermal degradation of PMPDI during ALD. Specifically, thermogravimetric analysis (TGA) confirmed the stability of PMPDI up to 400 °C (Figure S5), consistent with the generally reported thermal stability of PDI to approximately 300–600 °C,[14] so that the ≤200 °C used herein should not be a problem unless there was efficient catalysis of PMPDI decomposition by the deposited AlO_x. This latter possibility was ruled out by a second control experiment demonstrating the unchanged optical absorption spectrum of a photoanode before and after the ALD at the elevated, up to 200 °C temperatures employed (Figure S2 of the Supporting Information). The interesting higher photocurrent observed from the AlO_x layer deposited at the *lower* temperature might be associated with the surface states at AlO_x being able to serve as mediators for the photocatalytic reaction, increasing the overall photocatalytic activity of PMPDI[28,52], an intriguing working hypothesis for going forward and possible further investigation.

In all cases, without the addition of catalyst, the photocurrents observed in the SnO_2/PMPDI/AlO_x systems are not attributable to water oxidation, consistent with the original SnO_2/PMPDI system.[10] We hypothesize that perhaps the photocurrent could be due to some combination of dye degradation (though dye losses are minimal and even full dye degradation cannot account for all charge passed)[10], oxidation of water to H_2O_2 and oxidation of trace impurities.

Incident-photon-to-current efficiency (IPCE) and Faradaic efficiency of SnO_2/PMPDI/AlO_x photoanodes

The IPCE of the optimized SnO_2/PMPDI/AlO_x (0.6 nm, 85 °C) was measured to examine the role of AlO_x layer in improving the photocurrent. An action spectrum of the photocurrent vs wavelength of incident light was collected in the presence of the two-electron, kinetically facile sacrificial reductant hydroquinone (H_2Q), $H_2Q \rightarrow Q^{2-} + 2H^+ + 2e^-$, Figure 6, left.

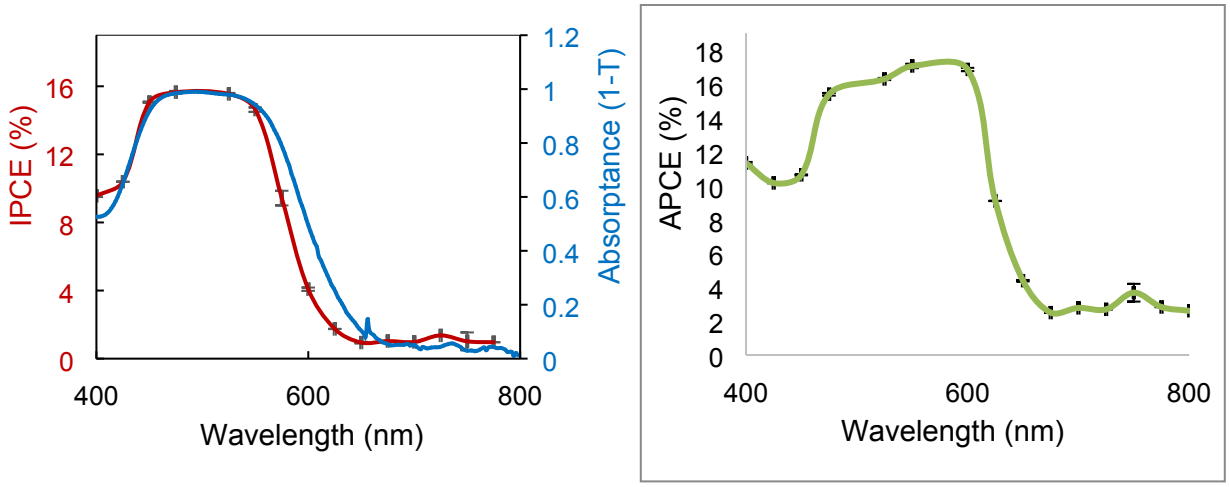

Figure 6. (left) IPCE spectrum of SnO_2/PMPDI/AlO_x (0.6 nm, 85 °C deposition) anode in pH 7, 0.1 M KPi buffer with 20 mM H_2Q sacrificial reductant (red) plotted along with the optical absorptance spectrum of PMPDI (blue) and (right) APCE spectra of SnO_2/PMPDI/AlO_x (0.6 nm, 85 °C deposition) anode in pH 7, 0.1 M KPi buffer with 20 mM H_2Q sacrificial reductant.

The IPCE spectrum measured with H_2Q resembles the optical absorptance spectrum of PMPDI dye with some deviation at around 400–450 nm, photocurrent presumably due to some direct absorbance of light by bandgap excitation of SnO_2.[10] By dividing the IPCE by the absorptance of PMPDI, the absorbed photon-to-current efficiency (APCE) was calculated, where the APCE is the internal quantum efficiency of the system, that is the combination of the efficiencies of charge transfer across the semiconductor-electrolyte interface times the charge-collection efficiency at the electrode. The observed APCE is ~18% for the SnO_2/PMPDI/AlO_x (0.6 nm) (Figure 6, right), hence modestly superior to those of SnO_2/PMPDI without AlO_x (APCE = ~13%), but ~2.5-fold superior to the original thin film system, indium doped tin oxide (ITO)/PMPDI with CoO_y WOC (APCE = ~6%)[9]. The observed, higher APCE indicates that more photocurrent is produced for the given number of absorbed photons when the AlO_x overlayer was applied, consistent with the hypothesis discussed: the AlO_x overlayer passivates the defect states at SnO_2 surface thereby reducing charge recombination while the surface states of AlO_x assist the photocatalytic reaction at the electrolyte interface.

Effects of the combined application of CoO_y WOC and AlO_x passivation layer

We tested if the combination of CoO_y WOC with ALD AlO_x passivation (1.3 nm, 85 °C) could lead to an additional enhancement in water oxidation photocurrent of the SnO_2/PMPDI

photoanode. As discussed above, previous reports have shown that the application of WOC to the DS-PEC system with metal oxide passivation layer led to an undesired *decrease* in the photocurrent outputs.[10,21]

We find that the photocurrent in our SnO_2/PMPDI/AlO_x/CoO_y photoanode in fact slightly *increased* over the SnO_2/PMPDI/CoO_y control, indicating that the particular AlO_x passivation layer does not interfere with the catalytic function of CoO_y WOC in our case (Figure 7a). Specifically, we observe that the application of AlO_x increases the magnitude of steady-state photocurrent at a given potential for the system (e.g., from –15 μA/cm^2 to –19 μA/cm^2 at +0.9 V vs Ag/AgCl for SnO_2/PMPDI/CoO_y and SnO_2/PMPDI/AlO_x/CoO_y, respectively), while decreasing the extent of photocurrent spiking (e.g., at +0.2 V vs Ag/AgCl, 72% decay for SnO_2/PMPDI/AlO_x/CoO_y and 89% decay for SnO_2/PMPDI/CoO_y), consistent with the reduced charge recombination enabled by AlO_x passivation. An extended experiment looking at photocurrent decay in the optimized SnO_2/PMPDI/AlO_x/CoO_y was also carried out, showing approximately 78% decay in photocurrent after ca. 1.5 hours (Figure S7).

To the best of our knowledge, this result represents one of the first observations in which the photoanode passivation does not interfere with the activity of CoO_y WOC as compared to the system without the passivation layer deposited onto a PEC. However, the photocurrent from SnO_2/PMPDI/AlO_x/CoO_y photoanodes is still inferior to those of SnO_2/PMPDI/AlO_x counterparts *without* CoO_y WOC (Figure 7a), although the origin of the photocurrent from the latter case is still unknown, given that no catalyst or sacrificial reductant were added and no oxygen detected.

Decreasing the AlO_x thickness in the SnO_2/PMPDI/AlO_x/CoO_y photoanode further increases the photocurrent output (Figure 7b), similar to the discussed trend in SnO_2/PMPDI/AlO_x without CoO_y WOC. The sample with the thinnest, 0.6 nm AlO_x coating achieved the most photocurrent of –42 μA/cm^2 at +0.9 V vs Ag/AgCl, which is nearly 2.5 times higher than that obtained for SnO_2/PMPDI/CoO_y without any AlO_x overlayer.

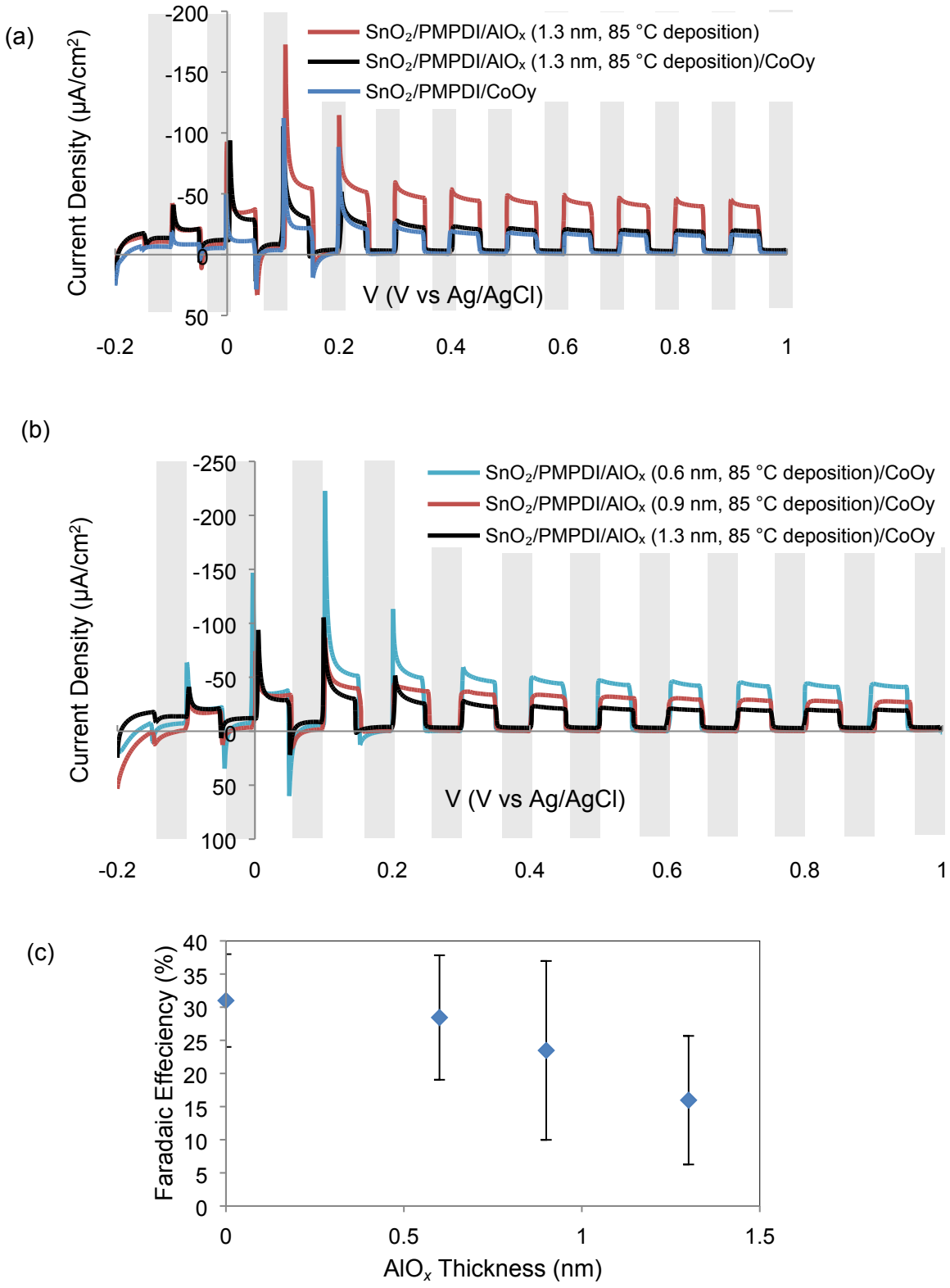

Figure 7. Photocurrent transients (indicated by light (light-on)/ dark (light-off) shading, 5 s each) collected in pH 7, 0.1 M KPi electrolyte for: (a) SnO_2/PMPDI/CoO_y (blue), SnO_2/PMPDI/AlO_x (1.3 nm, 85 °C deposition, red) and SnO_2/PMPDI/AlO_x/CoO_y (1.3 nm, 85 °C deposition, black) anodes; (b) SnO_2/PMPDI/AlO_x/CoO_x (0.6 nm, 85 °C

deposition, blue), SnO_2/PMPDI/AlO_x/CoO_y (0.9 nm, 85 °C deposition, red), and SnO_2/PMPDI/AlO_x/CoO_y (1.3 nm, 85 °C deposition, black) anodes; (c) Faradaic efficiency values for O_2 generation for SnO_2/PMPDI/AlO_x/CoO_y (85 °C AlO_x ALD) with varying AlO_x thicknesses. In all cases oxygen was produced and the Faradaic efficiency was found to be the comparable within error.

We further demonstrate the observed photocurrent is actually derived from water oxidation by measuring Faradic efficiency via the generator–collector (G-C) method[10,22–24,53] to detect quantitatively the amount of oxygen produced. We find that for all alumina passivation layer thicknesses, the Faradaic efficiency values were largely comparable (Figure 7c), with the photoanode passivated by 0.6 nm thick alumina displaying a Faradaic efficiency of 29 ± 9%. This value is within error of that measured from SnO_2/PMPDI/CoO_y without any AlO_x, and samples with thicker AlO_x showed slightly lower average Faradaic efficiencies, though also within error. All samples without catalyst displayed a Faradaic efficiency of 0% prior to CoO_y deposition. Of note, photocurrent decays in extended O_2 generation experiments, 20 minutes, resulted in ca. 11% decay in O_2 generation (S8).

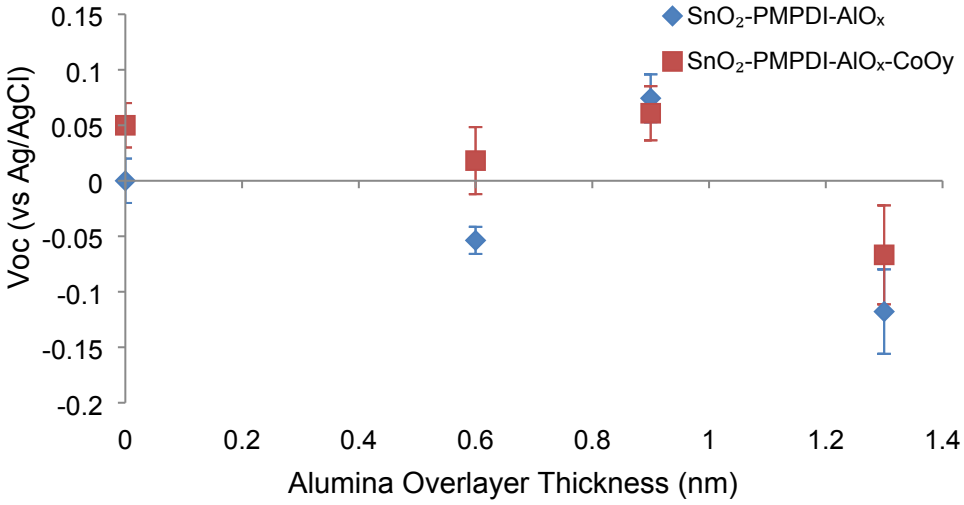

Figure 8. V_{oc} vs Ag/AgCl reference electrode in a half-cell setup for SnO_2/PMPDI/AlO_x (85 °C deposition, blue) and SnO_2/PMPDI/AlO_x (85 °C deposition)/CoO_y (red) anodes at differing AlO_x deposition thicknesses. In this case, $V_{oc} \approx E_{F,n}$, the quasi-Fermi energy of electrons in the SnO_2 sub-bandgap states.

We examined the effects of CoO_y WOC on the V_{oc} of SnO_2/PMPDI/AlO_x photoanode with varying AlO_x thickness to understand the impact of CoO_y WOC and AlO_x on the charge recombination and injection (Figure 8). When the SnO_2/PMPDI/AlO_x photoanode is illuminated under open circuit, the measured V_{oc} reflects the quasi-Fermi energy of electrons ($E_{F,n}$) in the nano-

SnO_2 substrate with respect to a reference electrode potential. The V_{oc} is determined by the steady-state charge-carrier concentration—that is, the quasi-equilibrium—set by the balance between the relative rates of the electron injection from the photoexcited dye to SnO_2 vs the depopulation of the SnO_2 states via recombination[10,54] (see Scheme 1, described in more detail below).

Since the addition of the CoO_y WOC in principle should not alter the electron injection rate from PMPDI, any shift in V_{oc} can be attributed to a change in the recombination rate for a given thickness of AlO_x passivation layer.[10,54] Based on the V_{oc} results (Figure 8, Table 1), we find a general trend that the measured magnitude of V_{oc} increases while being negative (i.e, the electron quasi-Fermi energy increases due to decreasing rates of recombination relative to injection) as AlO_x thicknesses increases. This result is as expected if AlO_x acts as a tunneling barrier to electrons leaving SnO_2. Furthermore, we find a general trend that the measured average V_{oc} is more positive (i.e., the electron quasi-Fermi energy is lower due to increasing rates of recombination relative to injection) after depositing the CoO_y WOC. This result suggests that the CoO_y is able to scavenge electrons from the SnO_2, despite the AlO_x tunneling barrier, which is consistent with the observed photocurrent results, where photocurrents always decreased for a given AlO_x thickness after depositing CoO_y. The samples with 0.9 nm thick AlO_x appear to be outliers from both trends, showing the most positive V_{oc} (most recombination) and negligible effect of CoO_y on V_{oc} within error. The changing kinetics of the system with differing amounts of alumina reflect the complexity of the kinetics herein, both an advantage and disadvantage of adding a component to a system.

Alumina Thickness (nm)	**Voc Without CoO_y vs Ag/AgCl**	**Voc With CoO_y vs Ag/AgCl**
0	0 ± 0.02	0.05 ± 0.02
0.6	-0.054 ± 0.01	0.018 ± 0.03
0.9	0.074 ± 0.02	0.061 ± 0.02
1.3	-0.12 ± 0.04	-0.067 ± 0.04

Table 1. Open circuit voltage vs Ag/AgCl for varying thicknesses of alumina deposition with and without CoO_y catalyst addition. The addition of CoO_y either increases V_{oc} (0 nm and 0.6 nm of AlO_x) or induces a negligible change (0.9 nm and 1.3 nm AlO_x).

Scheme 1. Hypothesized kinetic scheme of the SnO_2/PMPDI/AlO_x/CoO_y system where SnO_2 is grey, PMPDI is pink, AlO_x is blue, and CoO_y is yellow. Green arrows indicate idealized pathways for charge transfer in WOC. Red arrows indicate loss of efficiency in the form of charge-carrier recombination. Arrows to the AlO_x are not included in this scheme based on the assumption that the ultrathin AlO_x is a tunneling barrier in which no charge carrier accumulation

occurs. The lack of charge transfer pathways to or from the AlO_x energy states indicates that, qualitatively, the charge transfer pathways of the system with and without AlO_x would be identical; that is, the arrows depicted in a kinetic scheme of the anode would be the same.

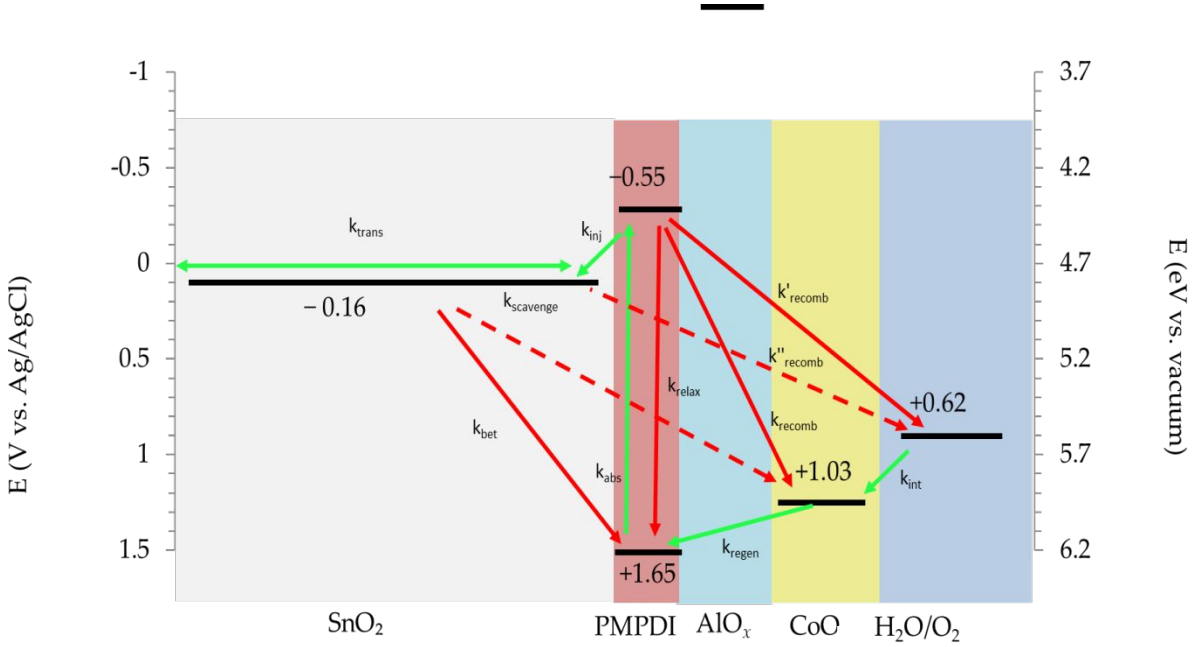

A kinetic scheme, Scheme 1, was constructed in order to better illustrate and understand how charge transfer occurs throughout the SnO_2/PMPDI/AlO_x/CoO_y device. Kinetic pathways were identified using k_{trans}, $k_{scavenge}$, k_{inj}, k_{recomb}, k_{abs}, and k_{relax} indicating electron transfer, injection, recombination, absorbance, and relaxation, respectively. This idealized, deliberately minimalistic scheme shows the kinetic pathways for the system in which defects and impurities are not present. The V_{oc} results summarized in Table 1 above can be rationalized by postulating recombination between SnO_2 to CoO_y, as depicted in Scheme 1 by the red dashed arrow from the SnO_2 conduction band energy level at −0.16 V vs Ag/AgCl to CoO_y (with a catalytic onset potential of +1.03 V vs Ag/AgCl).

What is not represented in the kinetic scheme but is crucially important to understanding recombination and efficiency in a WOCatalysis system is the changes in the rate constants for each charge transfer pathway that passes through the AlO_x 'blocking' layer. In the case of 1.3 nm thick AlO_x, the V_{oc} is lowest (i.e., most negative), indicating a lowered charge recombination, postulated to be due to a larger tunneling barrier between SnO_2 and CoO_y. Given that 1.3 nm thick AlO_x also

results in the lowest amount of photocurrent, this suggests that the comparatively thicker AlO_x passivation layer also slows electron transfer from the CoO_y catalyst to regenerate the photo-oxidized PMPDI, or slows electron transfer from photo-excited PMPDI to SnO_2. The latter effect is less likely, because the AlO_x overlayer was deposited after PMPDI. Hence, while valuable for beginning to understand the present system in better kinetic detail, future studies testing the pathways in Scheme 1 and measuring rate constants will be needed to better understand in detail how and why the addition of the AlO_x layer improves photocurrent in the present system.

Structural model for AlO_x passivation layer and CoO_y WOC

A typical assumption in the dye-sensitized solar cell (DSSC) and DS-PEC literature is that ALD surface treatments are able to uniformly coat the entire interior surface area of a mesoporous metal oxide. However, the AlO_x passivation layer prepared by the ALD protocol used in this study was likely unable to produce a fully conformal coating on the PMPDI loaded throughout the bulk of 4 μm-thick mesoporous SnO_2. The ALD process, similar to chemical vapor deposition in nature, relies on an efficient transport of vapor-phase precursors to a target surface on which materials are deposited. Unlike flat substrates, three-dimensional (3D) mesoporous substrates require significantly longer time for the precursors to be able to diffuse into the mesopores (i.e., Kundsen diffusion) to generate a fully conformal coating throughout the bulk interior of the mesopores. In our ALD process, the PMPDI-loaded mesoporous SnO_2 was exposed to materials precursors (either TMA or water) for 1 min during each cycle under dynamic vacuum (i.e., continuous evacuation of the chamber under constant flow of background carrier gas (nitrogen; 20 sccm)). That treatment is not expected to allow diffusion of precursors deep into the bulk of mesoporous SnO_2 film. The resulting AlO_x passivation layer should, then and in turn, be covering mostly only the upper portion of mesoporous SnO_2 film.

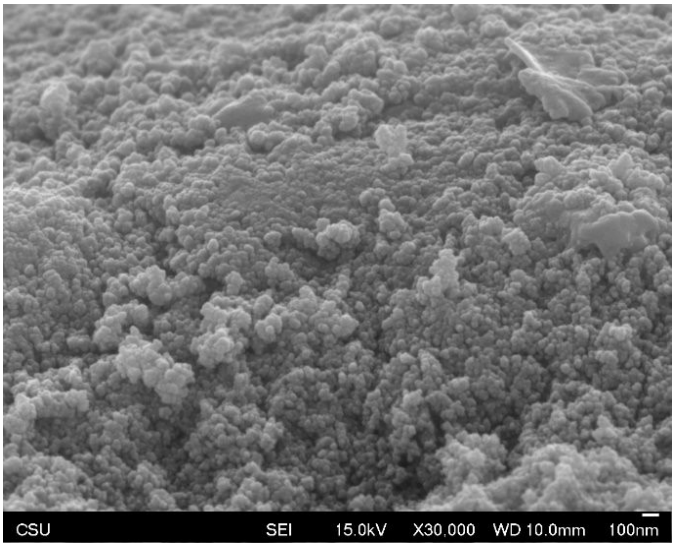

Figure 9: SEM image of SnO_2/PMPDI/AlO_x (0.6 nm, 85 °C)/CoO_y anode taken at 30,000X magnification.

An artistic representation of the SnO_2/PMPDI/AlO_x/CoO_y anode system developed and examined herein was created based on scanning electron microscopy (SEM) imaging of the anodes (Figure 9). This rendering (Figure 10) is based on a series of SEM images of the anodes, both with alumina (Figure 9) and previously published[10], showing the distinctly nanostructured features reflected in this depiction. Understanding the layering and interaction of each component is necessary to accurately examine the kinetics of the system as a whole.

For the thinner AlO_y coatings employed, we illustrate a hypothesized thin surface coating at the outer most surface of the SnO_2 only (Fig. 10a). The subsequent application of the CoO_y WOC onto the anode structure likely results in CoO_y directly in contact with PMPDI, and SnO_2, within the deeper portion of mesoporous SnO_2 film, as opposed to the CoO_y placed on AlO_x overlayer at the upper region of the SnO_2 film. This is consistent with the observed increased charge recombination and, consequently, reduced photocurrent output for the full system with added CoO_y. Attempts to determine the location and prevalence of cobalt using SEM- energy dispersive X-ray spectrometer (EDS) and XPS were unsuccessful due to the very low, catalytic quantities of CoO_y used (for further discussion see S5 and S7). Although the CoO_y catalyst was not visible by XPS, alumina is present in the anodes according to XPS (Figure S4).

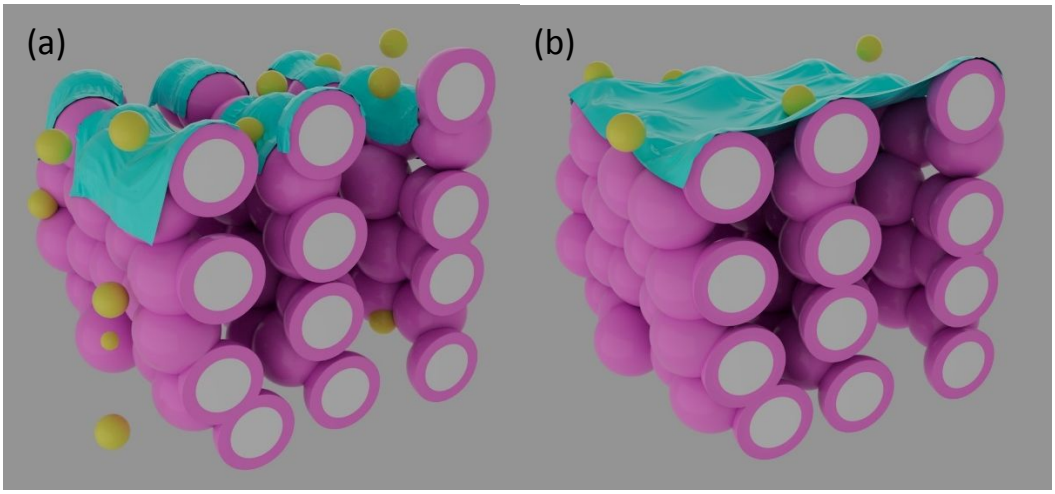

Figure 10. Idealized structural models of the SnO_2/PMPDI/AlO_x/CoO_y anode with (a) 0–0.9 nm thick AlO_x layer and (b) 1.3 nm thick or greater AlO_x layer, where SnO_2 is grey, PMPDI is pink, AlO_x is blue, and CoO_y is yellow. Note that in (b) a full, impenetrable coverage by the alumina over the SnO_2 surface is implied, and therefore no yellow CoO_y is shown in the lower part of (b). Structural models are based on SEM imaging of anodes, which showed distinct nanostructured behavior as rendered herein.

As for the 1.3-nm-thick AlO_x layer, the passivation now may be thick enough to more thoroughly cover at least some of the mesopores, more similar to Figure 10b than 10a, preventing at least some direct contact between SnO_2 and CoO_y as can happen with the ultrathin, 0.6 nm layer for example, so that recombination is not increased (or at least not as much) following the application of CoO_y. But, the thicker AlO_x passivation layer has other effects, as already noted, inhibiting the efficiency of necessary electron transfer from the CoO_y to PMPDI, while also preventing the full utilization of PMPDI loaded within the bulk of mesoporous SnO_2 film. The net effect of the even modestly thicker AlO_x layer is that the performance of base SnO_2/PMPDI/AlO_x, 0.6 nm thickness AlO_x, anode is overall reduced.

Conclusions

In the present study we have examined a SnO_2/PMPDI DS-PEC system for photoelectrochemical water oxidation catalysis where an ultrathin AlO_x passivation layer is added by low-temperature ALD, with and without a CoO_y WOC. The thickness- and deposition-temperature parameters of the ALD were explored with the goal of optimizing the system. The answers obtained to the four primary questions posed at the start of the studies are the following: (i) *yes*, deposition of an ultrathin alumina overlayer applied by ALD on the PMPDI/SnO_2

photoanode can improve the photoactivity and catalytic activity of the system; (ii) *yes*, perhaps surprisingly as one of the more interesting results of the present study, the addition of specifically a ~1-nm-thick AlO_x layer deposited on a *4000 nm (i.e., 4 micron) thick mesoporous* anode system can and does have a positive, 2.5-fold improvement in the steady-state photocurrent with 29 ± 9% Faradaic efficiency vs the control anode without alumina passivation. Reduced charge-carrier recombination explains the observed effect. Next, (iii) *yes*, layer thickness and deposition temperature of the alumina overlayer are key parameters, a 0.6-nm-thick AlO_x layer deposited at 85 °C providing the best photocatalytic activity in our hands; so that (iv) *yes*, ALD- deposited, ultrathin AlO_x layers is a useful tool to address the carrier recombination in nanostructured/dye systems such as SnO_2/PMPDI DS-PECs. Additionally, (v) *yes*, ALD-deposited AlO_x layer does help support the understanding of the "anti-catalysis" of co-depositing a CoO_y WOC on the SnO_2/PMPDI DS-PECs—specifically the picture of direct CoO_y–SnO_2 contact-mediated recombination—but was unable to improve the photocurrent in a net SnO_2/PMPDI/AlO_x(/CoO_y) system. The results document that metal-oxide passivation by low-temperature ALD can be an effective strategy for improving the water oxidation performance of even nanostructured DS-PECs. The results indicate that further optimizing the ALD protocol by tailoring it towards mesoporous structures—for example, by utilizing the ALD-derived infiltration synthesis method[55,56]—merits experimental testing.

Overall, we find the addition of an optimized *ultrathin* AlO_x layer (0.6 nm thick; deposited at 85 °C) improves the SnO_2/PMPDI/AlO_x system's photoactivity by a factor of up to ~3-fold with reduced recombination. However, the addition of CoO_y still results in a decrease in photoactivity compared to the SnO_2/PMPDI/AlO_x system without CoO_y, but a Faradaic efficiency of oxygen production of ca. 30%. We attribute the lack of a performance enhancement by CoO_y WOC to incomplete coverage of each SnO_2 nanoparticle by the AlO_x. Despite the decrease in photoactivity with the addition of the CoO_y WOC, the SnO_2/PMPDI/AlO_x/CoO_y system yields a higher photocurrent in all cases compared to the original, alumina-free SnO_2/PMPDI/CoO_y system.

Associated Content

Supporting Information

The Supporting Information is available free of charge at

Author Information

Corresponding Author

*Richard.Finke@colostate.edu; cynam@bnl.gov

Acknowledgements

This research was supported by the National Science Foundation under Grant No. 1664646. The authors thank the members of Prof. Finke's research group and Dr. Joel Kirner for reading draft versions of this manuscript and providing valuable feedback. Additional thanks to Audrey Jewell for production of artistic renderings. This research used resources of the Center for Functional Nanomaterials, which is a U.S. DOE Office of Science Facility, at Brookhaven National Laboratory under Contract No. DE-SC0012704.

References

(1) Smalley, R. E. Future Global Energy Prosperity: The Terawatt Challenge. *Mater. Matters* **2004**, *30*, 412–417.

(2) Lewis, N. S.; Nocera, D. G. Powering the Planet: Chemical Challenges in Solar Energy Utilization. *Proc. Natl. Acad. Sci. U. S. A.* **2006**, *103*, 15729–15735.

(3) Kudo, A.; Miseki, Y. Heterogeneous Photocatalyst Materials for Water Splitting. *Chem. Soc. Rev.* **2009**, *38*, 253–278.

(4) Kirner, J. T.; Finke, R. G. Water-Oxidation Photoanodes Using Organic Light- Harvesting Materials: A Review. *J. Mater. Chem. A* **2017**, *5*, 19560–19592.

(5) Tachibana, Y.; Vayssieres, L.; Durrant, J. R. Artificial Photosynthesis for Solar Water-Splitting. *Nat. Photonics* **2012**, *6*, 511–518.

(6) Swierk, J. R.; Mallouk, T. E. Design and Development of Photoanodes for Water-Splitting Dye-Sensitized Photoelectrochemical Cells. *Chem. Soc. Rev.* **2013**, *42*, 2357–2387.

(7) Roger, I.; Shipman, M. A.; Symes, M. D. Earth-Abundant Catalysts for Electrochemical and Photoelectrochemical Water Splitting. *Nat. Rev. Chem.* **2017**.

(8) Law, K. Y. Organic Photoconductive Materials: Recent Trends and Developments. *Chem. Rev.* **1993**, *93*, 449–486.

(9) Kirner, J. T.; Stracke, J. J.; Gregg, B. A.; Finke, R. G. Visible-Light-Assisted Photoelectrochemical Water Oxidation by Thin Films of a Phosphonate-Functionalized Perylene Diimide Plus CoO_x Cocatalyst. *ACS Appl. Mater. Interfaces* **2014**, *6*, 13367–13377.

(10) Kirner, J. T.; Finke, R. G. Sensitization of Nanocrystalline Metal Oxides with a Phosphonate- Functionalized Perylene Diimide for Photoelectrochemical Water Oxidation with a CoO_x Catalyst. *ACS Appl. Mater. Interfaces* **2017**, *9*, 27625–27637.

(11) Mariotti, N.; Bonomo, M.; Fagiolari, L.; Barbero, N.; Gerbaldi, C.; Bella, F.; Barolo, C. Recent Advances in Eco-Friendly and Cost-Effective Materials towards Sustainable Dye-Sensitized Solar Cells. *Green Chem.* **2020**, *22*, 7168–7218.

(12) Carella, A.; Borbone, F.; Centore, R. Research Progress on Photosensitizers for DSSC. *Front. Chem.* **2018**, *6*, 481.

(13) Shalini, S.; Balasundaraprabhu, R.; Kumar, T. S.; Prabavathy, N.; Senthilarasu, S.; Prasanna, S. Status and Outlook of Sensitizers/Dyes Used in Dye Sensitized Solar Cells (DSSC): A Review. *Int. J. Energy Res.* **2016**, *40*, 1303–1320.

(14) Pasaogullari, N.; Icil, H.; Demuth, M. Symmetrical and Unsymmetrical Perylene Diimides: Their Synthesis, Photophysical and Electrochemical Properties. *Dye. Pigment.* **2006**, *69*, 118–127.

(15) Bard, A. J.; Whitesides, G. M.; Zare, R. N.; McLafferty, F. W. Holy Grails in Chemistry. *Acc. Chem. Res.* **1995**, *28*, 91.

(16) Kanan, M. W.; Nocera, D. G. In Situ Formation of an Oxygen-Evolving Catalyst in Neutral Water Containing Phosphate and Co^{2+}. *Science.* **2008**, *321*, 1072–1073.

(17) Prasittichai, C.; Hupp, J. T. Surface Modification of SnO_2 Photoelectrodes in Dye-Sensitized Solar Cells: Significant Improvements in Photovoltage via Al_2O_3 Atomic Layer Deposition. *J. Phys. Chem. Lett.* **2010**, *1*, 1611–1615.

(18) Swierk, J. R.; McCool, N. S.; Saunders, T. P.; Barber, G. D.; Mallouk, T. E. Effects of Electron Trapping and Protonation on the Efficiency of Water-Splitting Dye-Sensitized Solar Cells. *J. Am. Chem. Soc.* **2014**, *136*, 10974–10982. h

(19) Foundation, N. S. Catalytic Chemistry Workshop on Defining Critical Directions for the

Future; 2011; pp 1–20.

(20) Kay, A.; Grätzel, M. Dye-Sensitized Core-Shell Nanocrystals: Improved Efficiency of Mesoporous Tin Oxide Electrodes Coated with a Thin Layer of an Insulating Oxide. *Chem. Mater.* **2002**, *14*, 2930–2935.

(21) Kamire, R. J.; Materna, K. L.; Hoffeditz, W. L.; Phelan, B. T.; Thomsen, J. M.; Farha, O. K.; Hupp, J. T.; Brudvig, G. W.; Wasielewski, M. R. Photodriven Oxidation of Surface-Bound Iridium-Based Molecular Water-Oxidation Catalysts on Perylene-3,4-Dicarboximide-Sensitized TiO_2 Electrodes Protected by an Al2O3 Layer. *J. Phys. Chem. C* **2017**, *121*, 3752–3764.

(22) Zhao, Y.; Swierk, J. R.; Megiatto Jr, J. D.; Sherman, B.; Youngblood, W. J.; Qin, D.; Lentz, D. M.; Moore, A. L.; Moore, T. A.; Gust, D.; et al. Improving the Efficiency of Water Splitting in Dye-Sensitized Solar Cells by Using a Biomimetic Electron Transfer Mediator. *Proc. Natl. Acad. Sci. U. S. A.* **2012**, *109*, 15612–15616.

(23) Ashford, D. L.; Sherman, B. D.; Binstead, R. A.; Templeton, J. L.; Meyer, T. J. Electro-Assembly of a Chromophore-Catalyst Bilayer for Water Oxidation and Photocatalytic Water Splitting. *Angew. Chem. Int. Ed.* **2015**, *54*, 4778–4781.

(24) Sherman, B. D.; Sheridan, M. V; Dares, C. J.; Meyer, T. J. Two Electrode Collector−Generator Method for the Detection of Electrochemically or Photoelectrochemically Produced O_2. *Anal. Chem.* **2016**, *88*, 7076–7082.

(25) Hanson, K.; Losego, M. D.; Kalanyan, B.; Parsons, G. N.; Meyer, T. J. Stabilizing Small Molecules on Metal Oxide Surfaces Using Atomic Layer Deposition. *Nano Lett.* **2013**, *13*, 4802–4809.

(26) Donders, M. E.; Knoops, H. C. M.; Van De Sanden, M. C. M.; Kessels, W. M. M.; Notten, P. H. L.; Donders, M. E. Remote Plasma Atomic Layer Deposition of Co_3O_4 Thin Films. *J. Electrochem. Soc.* **2011**, *158*, 92–96.

(27) Klesko, J. P.; Kerrigan, M. M.; Winter, C. H. Low Temperature Thermal Atomic Layer Deposition of Cobalt Metal Films. *Chem. Mater.* **2016**, *28*, 700–703.

(28) Wang, L.; Yan, D.; Ye, X.; Liu, M.; Nam, C.-Y. Improved Stability and Performance of Visible Photoelectrochemical Water Splitting on Solution- Processed Organic Semiconductor Thin Films by Ultrathin Metal Oxide Passivation. *Chem. Mater.* **2018**, *30*, 342–335.

(29) Brennaman, M. K.; Dillon, R. J.; Alibabaei, L.; Gish, M. K.; Dares, C. J.; Ashford, D. L.; House, R. L.; Meyer, G. J.; Papanikolas, J. M.; Meyer, T. J. Finding the Way to Solar Fuels with Dye-Sensitized Photoelectrosynthesis Cells. *J. Am. Chem. Soc.* 2016, pp 13085–13102.

(30) Mccool, N. S.; Swierk, J. R.; Nemes, C. T.; Saunders, T. P.; Schmuttenmaer, C. A.; Mallouk, T. E. Proton-Induced Trap States, Injection and Recombination Dynamics in Water-Splitting Dye-Sensitized Photoelectrochemical Cells. *ACS Appl. Mater. Interfaces* **2016**, *8*, 16727–16735.

(31) Zazpe, R.; Prikryl, J.; Gä, V.; Nechvilova, K.; Benes, L.; Strizik, L.; Ales, Ger, J.; Bosund, M.; Sopha, H.; Macak, J. M. Atomic Layer Deposition Al_2O_3 Coatings Significantly Improve Thermal, Chemical, and Mechanical Stability of Anodic TiO2 Nanotube Layers. *Langmuir* **2017**, *33*, 3208–3216.

(32) Xu, P.; Mccool, N. S.; Mallouk, T. E. Water Splitting Dye-Sensitized Solar Cells. *Nano Today* **2017**, *14*, 42–58.

(33) Vandermolen, J.; Gomes, W.; Cardon, F. Investigation on the Kinetics of Electroreduction. *J. Electrochem. Soc.* **1980**, *10*, 2650–2651.

(34) Salvador, P.; Gutierrez, C. Mechanisms of Charge Transfer at the Semiconductor-Electrolyte Interface. *J. Electrochem. Soc.* **1984**, *131*, 326–336.

(35) Ondersma, J. W.; Hamann, T. W. Measurements and Modeling of Recombination from Nanoparticle TiO_2 Electrodes. *J. Am. Chem. Soc.* **2011**, *133*, 8264–8271.

(36) Weng, B.; Qi, M.-Y.; Han, C.; Tang, Z.-R.; Xu, Y.-J. Photocorrosion Inhibition of Semiconductor-Based Photocatalysts: Basic Principle, Current Development, and Future Perspective. *ACS Catal.* **2019**, *9*, 4642–4687.

(37) Kamire, R. J.; Majewski, M. B.; Hoffeditz, W. L.; Phelan, B. T.; Farha, O. K.; Hupp, J. T.; Wasielewski, M. R. Photodriven Hydrogen Evolution by Molecular Catalysts Using Al_2O_3-Protected Perylene-3,4-Dicarboximide on NiO Electrodes: The Design of Efficient Hydrogen-Evolving Photocathodes for Dye-Sensitized Photoelectrochemical Cells. *Chem. Sci.* **2017**, *8*, 541–549.

(38) Son, H.-J.; Prasittichai, C.; Mondloch, J. E.; Luo, L.; Wu, J.; Kim, D. W.; Farha, O. K.; Hupp, J. T. Dye Stabilization and Enhanced Photoelectrode Wettability in Water-Based Dye-Sensitized Solar Cells through Post-Assembly Atomic Layer Deposition of TiO_2. *J.*

Am. Chem. Soc. **2013**, *135*, 11529–11532.

(39) Michaux, K. E.; Gambardella, A. A.; Alibabaei, L.; Ashford, D. L.; Sherman, B. D.; Binstead, R. A.; Meyer, T. J.; Murray, R. W. Visible Photoelectrochemical Water Splitting Based on a Ru(II) Polypyridyl Chromophore and Iridium Oxide Nanoparticle Catalyst. *J. Phys. Chem. C* **2015**, *119*, 17023–17027.

(40) Lapides, A. M.; Sherman, B. D.; Brennaman, M. K.; Dares, C. J.; Skinner, K. R.; Templeton, J. L.; Meyer, T. J. Synthesis, Characterization, and Water Oxidation by a Molecular Chromophore-Catalyst Assembly Prepared by Atomic Layer Deposition. The "Mummy" Strategy. *Chem. Sci.* **2015**, *6*, 6398–6406.

(41) Kaeffer, N.; Massin, J.; Lebrun, C.; Renault, O.; Chavarot-Kerlidou, M.; Artero, V. Covalent Design for Dye-Sensitized H_2-Evolving Photocathodes Based on a Cobalt Diimine−Dioxime Catalyst. *J. Am. Chem. Soc.* **2016**, *138*, 12308–12311.

(42) Hamann, T. W.; Farha, O. K.; Hupp, J. T. Outer-Sphere Redox Couples as Shuttles in Dye-Sensitized Solar Cells. Performance Enhancement Based on Photoelectrode Modification via Atomic Layer Deposition. *J. Phys. Chem. C* **2008**, *112*, 19756–19764.

(43) Guo, J.; She, C.; Lian, T. Effect of Insulating Oxide Overlayers on Electron Injection Dynamics in Dye-Sensitized Nanocrystalline Thin Films. *J. Phys. Chem. C* **2007**, *111*, 8979–8987.

(44) Li, T. C.; Góes, M. S.; Fabregat-Santiago, F.; Bisquert, J.; Bueno, P. R.; Prasittichai, C.; Hupp, J. T.; Marks, T. J. Surface Passivation of Nanoporous TiO_2 via Atomic Layer Deposition of ZrO_2 for Solid-State Dye-Sensitized Solar Cell Applications. *J. Phys. Chem. C* **2009**, *113*, 18385–18390.

(45) Batra, N.; Gope, J.; Panigrahi, J.; Singh, R.; Singh, P. K. Influence of Deposition Temperature of Thermal ALD Deposited Al_2O_3 Films on Silicon Surface Passivation. *AIP Adv.* **2015**, *5*, 67113-1–5.

(46) Dingemans, G.; van de Sanden, M. C. M.; Kessels, W. M. M. Influence of the Deposition Temperature on the C-Si Surface Passivation by Al_2O_3 Films Synthesized by ALD and PECVD. *Electrochem. Solid-State Lett.* **2010**, *13*, H76–H79.

(47) Kukli, K.; Ritala, M.; Leskelä, M.; Jokinen, J. Atomic Layer Epitaxy Growth of Aluminum Oxide Thin Films from a Novel $Al(CH_3)_2Cl$ Precursor and H_2O. *J. Vac. Sci. Technol. A* **1997**, *15*, 2214–2218.

(48) Batra, N.; Gope, J.; Singh, R.; Panigrahi, J.; Tyagi, S.; Pathi, P.; Srivastava, S. K.; S Rauthan, C. M.; Singh, P. K. Effect of Low Thermal Budget Annealing on Surface Passivation of Silicon by ALD Based Aluminum Oxide Films. *Phys. Chem. Chem. Phys.* **2014**, *16*, 21804–21811.

(49) Rafí, J. M.; Zabala, M.; Beldarrain, O.; Campabadal, F. Deposition Temperature and Thermal Annealing Effects on the Electrical Characteristics of Atomic Layer Deposited Al_2O_3 Films on Silicon. *J. Electrochem. Soc.* **2011**, *158*, G108–G114.

(50) Groner, M. D.; Fabreguette, F. H.; Elam, J. W.; George, S. M. Low-Temperature Al_2O_3 Atomic Layer Deposition. *Chem. Mater.* **2004**, *16*, 639–645.

(51) Naumann, V.; Otto, M.; Wehrspohn, R. B.; Werner, M.; Hagendorf, C. Interface and Material Characterization of Thin ALD-Al_2O_3 Layers on Crystalline Silicon. *Energy Procedia* **2012**, *27*, 312–318.

(52) James Durrant, S. R.; Corby, S.; Laia FrancàsFrancàs, ab; Kafizas ab, A.; Durrant, J. R. Determining the Role of Oxygen Vacancies in the Photoelectrocatalytic Performance of WO_3 for Water Oxidation Determining the Role of Oxygen Vacancies in the Photoelectrocatalytic Performance of WO 3 for Water Oxidation. *Chem. Sci.* **2020**, *11*, 2907–2914.

(53) Sherman, B. D.; Sheridan, M. V; Wee, K.-R.; Song, N.; Dares, C. J.; Fang, Z.; Tamaki, Y.; Nayak, A.; Meyer, T. J. Analysis of Homogeneous Water Oxidation Catalysis with Collector−Generator Cells. *Inorg. Chem.* **2015**, *55*, 512–517.

(54) Ardo, S.; Meyer, G. J. Photodriven Heterogeneous Charge Transfer with Transition-Metal Compounds Anchored to TiO_2 Semiconductor Surfaces. *Chem. Soc. Rev.* **2009**, *38*, 115–164.

(55) Subramanian, A.; Tiwale, N.; Nam, C. Y. Review of Recent Advances in Applications of Vapor-Phase Material Infiltration Based on Atomic Layer Deposition. *JOM* **2019**, *71*, 185–196.

(56) McGuinness, E. K.; Zhang, F.; Ma, Y.; Lively, R. P.; Losego, M. D. Vapor Phase Infiltration of Metal Oxides into Nanoporous Polymers for Organic Solvent Separation Membranes. *Chem. Mater.* **2019**, *31*, 5509–5518.